Nanoscale

Accepted Manuscript

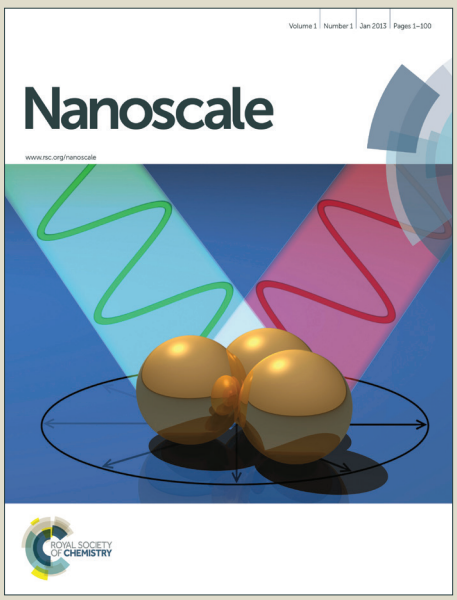

ROYAL SOCIETY OF CHEMISTRY

www.rsc.org/nanoscale

Cite this: DOI: 10.1039/c0xx00000x

www.rsc.org/xxxxxx

ARTICLE TYPE

Oxygen Vacancies Induced Selective Silver Deposition on the {001} Facets of BiOCl Single-Crystalline Nanosheets for Enhanced Cr(VI) and Sodium Pentachlorophenate Removal under Visible Light

Hao Li and Lizhi Zhang*

Received (in XXX, XXX) Xth XXXXXXXXX 20XX, Accepted Xth XXXXXXXXX 20XX
DOI: 10.1039/b000000x

We demonstrate that the high oxygen density characteristic of BiOCl {001} facets ensures the fast generation of oxygen vacancies in ethylene glycol under microwave irradiation, resulting in the in-situ nucleation and growth of Ag on the {001} facets of BiOCl single-crystalline nanosheets. The resulting Ag selectively deposited BiOCl single-crystalline nanosheets exhibit much higher reactivity and stability on both Cr(VI) reduction and sodium pentachlorophenate oxidation than the randomly deposited counterparts under visible light because of the tight contact between Ag and the {001} facets of BiOCl arisen from oxygen vacancies induced selective silver deposition.

Semiconductor photocatalysis has emerged as one of the most promising green and renewable technique for environmental treatment and remediation by harvesting the clean solar energy.[1-4] TiO_2 is the most used and studied photocatalyst because of its high activity, excellent stability, good biocompatibility and low cost. However, the wide-band-gap nature of TiO_2 (3.2 eV for anatase phase) limits its further application due to its poor response to visible light accounting for about 43% of solar light. Although many efforts have been made to enhance the photoreactivity of TiO_2 under visible light,[5-7] its photocatalytic performance is still far from the demand of practical applications. Since Awazu et al. innovatively employed the surface plasmon resonance effect of metallic nanostructures with enhanced ability to remove pollutants, "plasmonic phocatalysis" has become a promising strategy to enhance the visible light response of wide band-gap semiconductors like TiO_2 by either inducing near-field electromagnetic radiative energy to boost the generation of charge carriers within semiconductors,[8] or directly injecting surface plasmon resonance-excited energetic electrons to the conduction bands of semiconductors.[9] However, the catalytic performance and the stability of noble metal-semiconductor plasmonic photocatalytic systems suffer from the loose contact between noble metal and semiconductors synthesized with traditional colloidal methods arisen from the introduction of noble metal-stabilizing organic layer (surfactant or polymer),[10-12] resulting in low affinity and inefficient electron transfer between noble metal and semiconductor. Therefore, it is of great significance to prepare noble metal-semiconductor plasmonic photocatalysts with tight contact for efficient pollutant removal under visible light.

Recently Huang et al. developed a facile in-situ method to prepare metal/TiO_2 composites through redox reactions between electron-rich oxygen vacancies and metal salt. Later Ye et al. prepared urchin-like WO_3 nanostructure with significant amount oxygen vacancies to reduce noble metal ions onto the surface, resulting in metal-semiconductor composites with enhanced photoreactivity on the pollutant removal.[13] More recently, Xu et al. reported the Au-TiO_2 nanocomposites synthesized through in-situ oxygen vacancies induced metal reduction, which exhibited excellent photocatalytic stability.[14] Although these studies paved a new way for the synthesis of metal-semiconductor nanocomposits with tight contact in the absence of any foreign reducing or stabilizing agents, it is still unknown how the photocatalytic performances of the metal-semiconductor nanocomposites depend on the coupling modes of metal with certain facets of semiconductors. Since semiconductor crystal facets with different electronic structure, atomic arrangement, lattice symmetry, and spacing exhibit facet-dependent activity and selectivity in catalytic reactions,[15] it is high possible that the rational coupling of metal with certain facets of semiconductors in the nanocomposites can greatly enhance their reactivity and stability to remove pollutants under visible light, but seldom be explored.

Bismuth oxychloride (BiOCl) attracts more and more attention in the environmental field because of its typical layered structure with a self-built internal static electric field along [001] direction, which highly favors the separation of photo-induced charge carriers.[16] Recently, we reported the facet-dependent molecular oxygen activation property of BiOCl single-crystalline nanosheets (SCNSs) arisen from the surface atom exposure and the in situ-generated oxygen vacancy characteristics of the (001) and (010) surfaces under UV light irradiation.[17] Theoretically, the BiOCl {001} facets with a higher density of terminated oxygen atoms are more inclined to form oxygen vacancies than the {010} counterparts with a lower density of exposed oxygen atoms, possibly enabling the selective silver deposition on the BiOCl {001} facets via the oxygen vacancies induced silver reduction pathway. This oxygen vacancies induced silver selective deposition on the BiOCl {001} facets might establish a tight contact between Ag and {001} facets of BiOCl for efficient photocatalytic pollutant removal under visible light, which highly

deserves our investigation.

In this communication, we demonstrate that nanosized silver can be selectively deposited on the {001} facets of BiOCl SCNSs. The intrinsic reasons for the selective silver deposition on the {001} facets of BiOCl SCNSs are studied in details. The photocatalytic performance of the resulting silver selectively deposited on the {001} facets of BiOCl SCNSs is evaluated by the removal of two typical highly toxic pollutants of Cr(VI) and sodium pentachlorophenate (NaPCP) under visible light and also compared with that of the silver randomly deposited counterparts. The purposes of this study are to clarify the influence of coupling modes between metal and the facets of semiconductors on the photocatalytic activity of metal-semiconductor nanocomposites and to develop high performance plasmonic photocatalysts for efficient pollutant removal with solar energy.

Scanning electron microscopy (SEM) images revealed that the BiOCl with {001} facets exposed (BOC-001 SCNSs) possessed a well-defined decahedron shape with exposed {001} facets (Fig. 1a and 1b). The percentages of {001}, {111} and {110} facets were 71%, 25%, and 5%, respectively (Fig. 1c). The BiOCl with {010} facets exposed (BOC-010 SCNSs) were of a well-defined sheet-shaped structure with two exposed square {010} facets and four lateral {001} facets perpendicular to the {010} facets (Fig. 1d and 1e). The percentages of {010} and {001} facets were 77% and 23% (Fig. 1f), respectively. More detailed SEM, transmission electron microscopy (TEM), selected-area electron diffraction (SAED), high-resolution TEM (HRTEM) and X-ray diffraction (XRD) characterization results of the BOC-001 and BOC-010 SCNSs were provided in the supporting information (SI) (Fig. S1 and S2, ESI†).

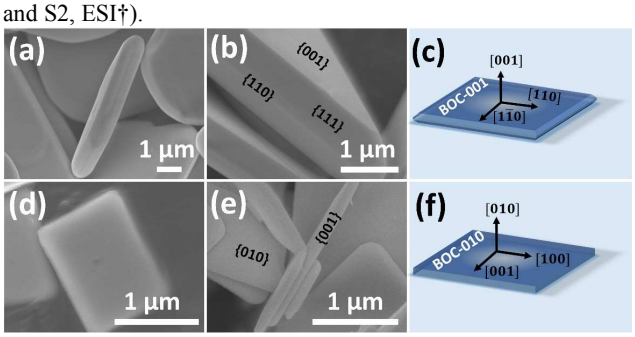

Fig. 1. (a), (b) SEM images and (c) schematic illustration of the crystal orientation of the BOC-001 SCNSs; (d), (e) SEM images and (f) schematic illustration of the crystal orientation of the BOC-010 SCNSs

A rapid microwave-assisted nonaqueous method was then adopted to selectively deposit silver onto the facets of BiOCl. After the microwave reactions of 10 min, many cube-like nanoislands with size up to 200 nm appeared on the top {001} facets of BOC-001 SCNSs (Fig. 2a, 2b, and S3a, ESI†), but no nanoparticle was observed on the dominating top {010} facets of BOC-010 SCNSs (Fig. S3b, ESI†). Surprisingly, abundant tiny nanoparticles of about 10 nm in sizes were found on the lateral {001} facets of BOC-010 SCNSs (Fig. 2c, 2d and S3c, ESI†), although the minor {001} facets of BOC-010 SCNSs merely accounted for 23% of total facets. Energy-dispersive X-ray spectrum (EDS) analysis revealed that the nanocubes and the nanoparticles on the {001} facets of BOC-001 and BOC-010 SCNSs were composed of metallic Ag (Fig. S4 and S5, ESI†). Two fitted individual peaks at 368.1 and 374.1 eV in the high-resolution Ag 3d XPS spectrum of Ag-BiOCl nanocomposites were assigned to the binding energies of Ag $3d_{5/2}$ and Ag $3d_{3/2}$ of metallic Ag, respectively (Fig. S6a, ESI†),[18] while the 6.0 eV difference between the above two binding energies was the typical characteristic of metallic Ag 3d state. HRTEM analysis confirmed the attachment of nanoparticles to the lateral facet of BOC-010 SCNSs, while the adjacent lattice fringes of 0.37 nm and 0.24 corresponded to the d spacing of (111) plane of face-centered-cubic (FCC) metallic Ag and (002) plane of tetragonal phase BiOCl (Fig. S3e, ESI†), respectively. All these observations revealed that nanosized silver were selectively deposited on the {001} facets of BiOCl single-crystalline nanosheets even with different facet exposure models. We therefore called Ag deposited BOC-001 and BOC-010 SCNSs as Ag-BOC-001 and Ag-BOC-010, respectively. The resulting Ag-BOC-001 and Ag-BOC-010 samples were further characterized with XRD analysis. A new peak at 38.2° corresponding to FCC metallic Ag appeared in the XRD pattern of Ag-BOC-001 (Fig. S6b, ESI†), while no peak of Ag could be observed in XRD pattern of Ag-BOC-010 because of its tiny amount (0.98 at%) as revealed by XPS analysis. The optical properties of the Ag-BiOCl composites were investigated with the UV-visible absorbance spectra (Fig. S6c, ESI†). Besides an absorption edge of defect-free BiOCl at 370 nm in the UV region, two new broad absorption band in the visible-light region were observed at 531 and 511 nm for Ag-BOC-001 and Ag-BOC-010, respectively, which are typical surface plasmon resonance (SPR) band absorption of metallic Ag.[19] Subsequent time dependent synthesis experiments revealed that the selective nucleation of silver on the top {001} facets of BOC-001 SCNS was much faster than that on the lateral {001} facets of BOC-010 SCNS (Fig. S7, ESI†). This result suggests that {001} facet exposure is crucial for the selective silver deposition and more {001} facet exposure favors the selective silver deposition in ethylene glycol under microwave irradiation.

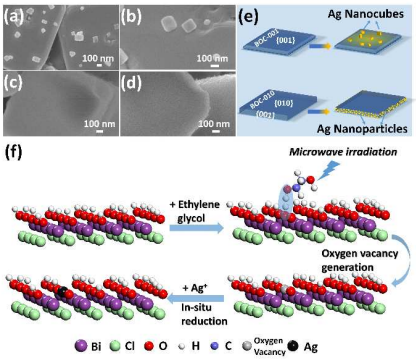

Fig. 2. (a) SEM images Ag-BOC-001 and (b) silver nanocubes on the top {001} facet of BOC-001; (c) SEM images of the Ag-BOC-010 nanosheets and (d) silver nanoparticles on the lateral {001} facet of BOC-010; (e) Schematic illustration of the silver deposition on the {001} facets of BOC-001 and BOC-010 SCNSs; (f) Possible pathway of the in situ reduction and deposition of Ag on the {001} facets of BiOCl in ethylene glycol under microwave irradiation.

Our previous theoretical calculation revealed that the oxygen atoms terminated {001} facets of BiOCl were stabilized by adsorbed hydrogen to form surface hydroxyl groups, while the {010} facets were free of adsorbed hydrogen.[17] To confirm the surface hydroxyl groups formation via the hydrogen adsorption on the terminated oxygen atoms of BiOCl {001} facets, we employed in-situ diffuse reflectance Fourier transform infrared

(FTIR) spectroscopy to probe the change of surface hydroxyl groups on the surface of BOC-001 and BOC-010 SCNSs along with temperature increase (Fig. S8 and S9, ESI†). In all cases, the signals of surface hydroxyl groups at 3560 cm^{-1} on the FTIR spectrum of BOC-001 SCNSs were much stronger than those of BOC-010 SCNSs, confirming that BOC-001 SCNSs with more terminated oxygen atoms possessed much more surface hydroxyl groups than BOC-010 SCNSs.

It is known that ethylene glycol molecules can react with BiOCl surfaces to remove the surface oxygen atoms, leaving over oxygen vacancies in the surface during the solvothermal reaction.[20] Meanwhile, ethylene glycol is also widely used as a typical solvent and reducing agent in noble metal synthesis with no selectivity involved.[21] To clarify the intrinsic reasons for the selective silver deposition on the {001} facets of BiOCl SCNSs, we first performed a control experiment by heating BOC-001 SCNSs and silver ions in ethylene glycol with the traditional solvothermal method, but failed to selectively deposit silver on any BiOCl facets (Fig. S10, ESI†). This result rules out the contribution of hot ethylene glycol induced direct silver ions reduction to the selective silver deposition, and also reveals that microwave heating is essential for the selective silver deposition in this study. We therefore hypothesize that microwave irradiation ensures the fast generation of oxygen vacancies in ethylene glycol, resulting in the in-situ nucleation of silver on the {001} facets of BiOCl SCNSs via the oxygen vacancies induced silver ions reduction, not the hot ethylene glycol induced silver ions reduction.

To confirm this opinion, we first checked the generation of oxygen vacancies in the BiOCl {001} facets by treating BOC-001 and BOC-010 SCNSs in ethylene glycol under microwave irradiation with a prolonged time. FTIR spectra analysis revealed that the decrease of surface hydroxyl groups of BOC-001 SCNSs was much more than that of BOC-010 SCNSs along with microwave treatment (Fig. S11a, ESI†). Moreover, BOC-001 SCNSs underwent a slight color change after being reacted with ethylene glycol under microwave irradiation (Fig. S11b, ESI†), as reflected by the appearance of a weak absorption tail in the visible light region of UV-vis absorption spectra (Fig. S11c, ESI†). This weak absorption tail arose from the absorption of surface oxygen vacancies.[22] These observations revealed that more oxygen vacancies could be generated in the {001} facets of BOC-001 SCNSs because of their higher {001} facet exposure. The generation of oxygen vacancies was further confirmed by the typical electron paramagnetic resonance (EPR) signal at g = 2.001 (Fig. S11d, ESI†).[23] Subsequently, we compared the generation of oxygen vacancies in the BiOCl {001} facets under microwave irradiation with the case of traditional solvothermal treatment. As expected, oxygen vacancies were not produced in the BiOCl {001} facets under solvothermal treatment with the same reaction temperature and duration time (Fig. S11d, ESI†), confirming the indispensable role of microwave irradiation in the fast generation of oxygen vacancies in ethylene glycol. We therefore conclude that the fast generation of oxygen vacancies in the BiOCl {001} facets in ethylene glycol under microwave irradiation is vital for the selective silver deposition on the BiOCl {001} facets (Fig. S11e, ESI†), which can avoid the unselective silver deposition caused by the hot ethylene glycol reduction.

To further verify the above point of view, the chemical reduction of silver ions with a typical reducing agent sodium borohydride was used to simulate the hot ethylene glycol induced silver ions reduction under microwave irradiation without generating oxygen vacancies. As expected, metallic Ag nanoparticles were randomly deposited on all the facets of BOC-001 and BOC-010 SCNSs without any selectivity (Fig. S12a, S12b, S12c and S12d, ESI†). Another control experiment was then conducted by replacing ethylene glycol with distilled water for the synthesis of Ag-BiOCl composites under microwave irradiation to check the role of ethylene glycol. The nonoccurrence of Ag deposition on the facets of BOC-001 and BOC-010 SCNSs in distilled water confirmed the indispensable role of ethylene glycol on the generation of oxygen vacancies and the subsequent deposition of silver nanostructures (Fig. S12e and S12f, ESI†). The oxygen vacancies induced silver ions reduction was also proven by the successful deposition of silver nanoparticles on the BiOCl {001} facets via directly reacting silver ions with BOC-001 SCNSs of oxygen vacancies in ethylene glycol at room temperature (Fig. S12g and S12h, ESI†).

On the basis of our experimental results and analyses, we propose a possible selective silver deposition pathway on the BiOCl {001} facets (Fig. 2f). Compared with the {010} facets of BiOCl, its {001} facets possess a higher density of surface terminated oxygen atoms. Under microwave irradiation, ethylene glycol could fast react with the {001} facets of BiOCl to remove the surface oxygen atoms and then eliminate surface hydroxyl groups, simultaneously resulting in oxygen vacancies selectively formed in the {001} facets. Once the silver ions reached the electron-rich oxygen vacancies, they were immediately reduced by the oxygen vacancies and then nucleated on the {001} facets, accompanying with the quenching of oxygen vacancies and the appearance of tight interfaces between the Ag and BiOCl surface. After nucleation, nanosized silver would further grow into nanocubes or nanoparticles on the {001} facets of BiOCl via the hot ethylene glycol induced silver ions reduction.

Both Cr(VI) and NaPCP are highly toxic contaminants commonly appeared in the wastewater and the surface water. To clarify the influence of coupling modes between silver and the facets of BiOCl SCNSs on their plasmonic photocatalytic activity, the silver nanostructures selectively deposited on the {001} facets of BiOCl SCNSs were used to remove Cr(VI) and NaPCP under visible light. As BiOCl with a wide indirect-transition optical bandgap of about 3.3 eV could not be directly excited under visible light, two kinds of bare BiOCl SCNSs showed no activity towards both Cr(VI) reduction and NaPCP oxidation (Fig. 3a and 3b) as well as poor transient photocurrent response under visible light (Fig. 3c). In contrast, Ag-BOC-001 could remove 65% of Cr(VI) and 62% of NaPCP, while the Ag-BOC-010 could remove 86% of Cr(VI) and 80% of NaPCP in 3 hours (Fig. 3a and 3b). This reveals that the nanosized silver selectively deposited on the {001} facets of BiOCl SCNSs can dramatically enhance their visible light photocatalytic reactivity. Interestingly, the pseudo-first-order kinetic constants of Ag-BOC-010 for both Cr(VI) reduction and NaPCP oxidation were respectively 1.9 and 1.7 times than those of Ag-BOC-001 under visible light (Fig. 3d), while Ag-BOC-010 also exhibited higher transient photocurrent response than Ag-BOC-001, although the absorption intensity of

Ag-BOC-010 in the visible light region was significantly weaker than that of Ag-BOC-001 (Fig. S6c, ESI†). The higher photoreactivity and transient photocurrent response of Ag-BOC-010 with a weaker absorption intensity in visible light region than those of Ag-BOC-001 with a stronger absorption intensity suggests that the smaller size of silver particles is more crucial for the transfer of SPR excited electrons to the {001} facets of BiOCl SCNSs in this study.

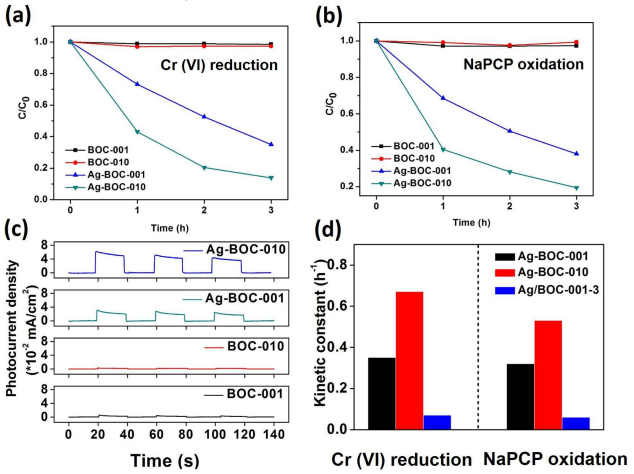

Figure 3. (a) Cr(VI) reduction and (b) NaPCP oxidation of the Ag-BOC-001 and Ag-BOC-010 nanocomposites under visible light. (c) Transient photocurrent responses of BOC-001, BOC-010, Ag-BOC-001 and Ag-BOC-010 SCNSs under visible light; (d) Comparison of the kinetic constants of the Ag-BOC-001, Ag-BOC-010, and Ag/BOC-001-3 nanocomposites for Cr(VI) reduction and NaPCP oxidation under visible light.

We subsequently prepared some counterpart samples by unselectively loading silver on the facets of BiOCl SCNSs with a sodium borohydride reduction method. As the precise synthesis of Ag/BOC-001-x composites of designed weight ratios of Ag to BiOCl with $NaBH_4$ reduction method was impossible, we thus prepared a series of Ag/BOC-001-x (x = 0.5, 1, 3 and 5) composites with Ag unselectively deposited on {001} facets of BiOCl. Although the random silver loading could also enhance the visible light photoreactivity of BiOCl SCNSs to some degree (Fig. S13a and S13b, ESI†), the best photoreactivity of the silver randomly deposited counterparts (3 wt% of Ag loading, Ag/BOC-001-3) was still far inferior to those of Ag-BOC-001 and Ag-BOC-010 (Fig. 3d). The pseudo-first-order kinetic constants of Ag-BOC-001 and Ag-BOC-010 for both Cr(VI) reduction and NaPCP oxidation were about 5 and 9 times those of Ag/BOC-001-3, respectively (Table S1, ESI†). Similarly, the transient photocurrents of the Ag/BOC-001-x composites enhanced slightly, but much weaker than those of the selective Ag-BOC-001 and Ag-BOC-010 composites (Fig. S13c and S13d, ESI†). Compared with Ag/BOC-001-x, the photocatalytic activity enhancement of Ag/BOC-010-x was less significant for the removal of Cr(VI) and NaPCP, which was probably ascribed to their different facet exposure (Fig. S13e and S13f, ESI†). Moreover, the further treatment of Ag/BOC-001-3 in ethylene glycol with microwave irradiation could not enhance its photoreactivity (Fig. S14, ESI†). These comparisons suggested the in-situ oxygen vacancies reduction method might induce a tighter contact between Ag and the {001} facets of BiOCl SCNSs than the sodium borohydride reduction method. Obviously, the tight contact between Ag and the facets of BiOCl SCNSs favors the transfer of SPR-excited electrons, which is the intrinsic reason for the superior pollutant removal performance of silver deposited on the {001} facets of BiOCl SCNSs under visible light.

To confirm the tight contact between Ag and the {001} facets of BiOCl SCNSs induced by the in-situ oxygen vacancies reduction method, we therefore compared the stability and reusability of the silver selectively deposited on the {001} facets of BiOCl SCNSs with that of the silver randomly deposited counterparts on the Cr(VI) reduction under visible light. As shown that, the photoreactivity of Ag-BOC-001 and Ag-BOC-010 on the Cr(VI) reduction did not decline even after five circles, indicating their excellent stability for environmental application (Fig. 4a and 4b). However, as for the silver randomly deposited counterpart of Ag/BOC-001-3, its efficiency decreased to about 30% of the initial value after five circles of photocatalytic Cr(VI) removal (Fig. 4c). This removal efficiency decrease might be attributed to the oxidation and/or the loss of the metallic Ag on the facets of BiOCl during the photocatalytic reaction, which was further analyzed by measuring the SPR absorption band of Ag nanoparticles in visible light region. As reflected in Fig. 4d and 4e, the SPR absorption bands of two Ag selectively deposited on the BiOCl (Ag-BOC-001 and Ag-BOC-010) did not change after multiple Cr(VI) removal experiments. In contrast, the intensity of SPR absorption band of Ag/BOC-001-3 weakened significantly although its shape and position were maintained (Fig. 4f). This indicated that the removal efficiency decrease of the silver randomly deposited sample was ascribed to the loss of Ag nanoparticles randomly deposited on the BiOCl surface, rather than the oxidation of surface metallic Ag nanoparticles. EDS analysis revealed that the molar ratio of Ag/Bi in Ag/BOC-001-3 decreased 65.8% after five circles of photocatalytic Cr(VI) removal, which was much higher than the values (8.8% and 9.0%) of Ag-BOC-001 and Ag-BOC-010 (Table S2, ESI†). The significant differences further confirmed the loss of Ag nanoparticles randomly deposited on the BiOCl surface during the photocatalysis process because of their loose contact. XRD analysis revealed that the as-prepared Ag-BOC-001 and Ag-BOC-010 exhibited no significant change after the 5th cycle of use and the intensity ratios of (002) and (020) peaks (Fig. S15, ESI†), confirming that the tight contact between Ag and the {001} facets of BiOCl SCNSs arisen from oxygen vacancy induced metal reduction can greatly enhance both the reactivity and the stability of the Ag-BiOCl plasmonic photocatalysts.

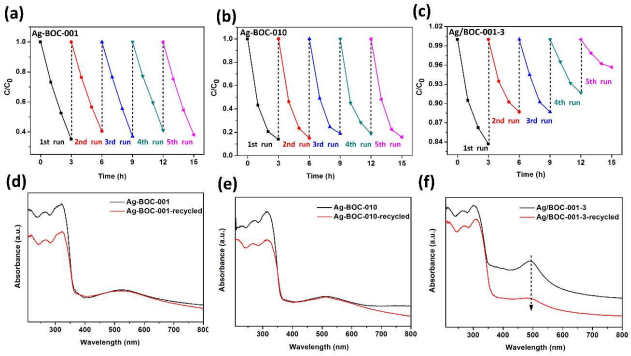

Figure 4. Recycled photoreduction of Cr(VI) over (a) Ag-BOC-001, (b) Ag-BOC-010, (c) Ag/BOC-001-3 and (d, e, f) the corresponding UV-visible absorbance spectra change after five times of recyclability test.

A series of experiments were then carried out to investigate the active species responsible for the Cr(VI) reduction and the NaPCP oxidation on the silver selectively deposited on the {001} facets of BiOCl SCNSs (Ag-BOC-010) with adding different kinds of excess scavengers (CCl_4 for electrons, tert-butyl alcohol for •OH, p-benzoquinone for $•O_2^-$, and $Na_2C_2O_4$ for holes) (Fig. S16, ESI†). As shown in Fig. 5a, the Cr(VI) photoreduction on Ag-BOC-010 was greatly suppressed by the addition of CCl_4, but hardly inhibited by tert-butyl alcohol (TBA). This indicated that photogenerated electrons mainly accounted for the Cr(VI) reduction. When Ar gas was purged to remove the molecular oxygen, Cr(VI) photoreduction was also suppressed. This suggested that superoxide radicals might be involved in the Cr(VI) photoreduction,[24] which was further confirmed by the significant Cr(VI) photoreduction suppression after the addition of p-benzoquinone. Therefore, we conclude that both photogenerated electrons and superoxide radicals contribute to the Cr(VI) reduction on Ag-BOC-010 under visible. Subsequently, we found that the addition of sodium acetate or p-benzoquinone or purging Ar gas greatly suppressed the NaPCP oxidation on Ag-BOC-010, but the NaPCP oxidation was not influenced by the addition of TBA (Fig. 5b). These results revealed the NaPCP oxidation were mainly attributed to holes and superoxide radicals generated by Ag-BOC-010 under visible light.

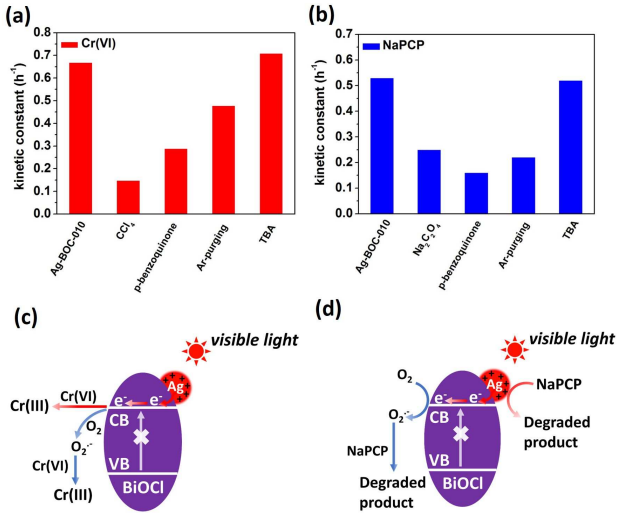

Figure 5. (a) Photocatalytic reduction of Cr(VI) and (b) oxidation of NaPCP over Ag-BOC-010 in the presence of different scavengers. Proposed (c) Cr(VI) reduction and (d) NaPCP oxidation processes of the Ag-BOC-001 and Ag-BOC-010 nanocomposites under visible light.

On the basis of the above results and discussion, the Cr(VI) reduction and the NaPCP oxidation on the silver selectively deposited on the {001} facets of BiOCl SCNSs under visible light could be proposed as follows (Fig. 5c and 5d). Under visible light irradiation, SPR-excited electrons would first enrich on the surface of nanosized Ag and then efficiently inject to the conduction band of BiOCl because of their tight contact arisen from oxygen vacancy induced metal reduction, leaving over holes to oxidize organic pollutants like NaPCP on nanosized Ag. After reaching the {001} facets of BiOCl SCNSs, the electrons would reduce Cr(VI) into Cr(III), or react with molecular oxygen to produce superoxide radicals because of the more negative conduction band potential of BiOCl than that of $O_2/•O_2^-$.[16] The generated superoxide radicals would then either reduce Cr(VI) or react with NaPCP.

Besides the efficient removal of Cr(VI) and the mineralization of NaPCP (Fig. S17, ESI†), the resulting Ag selectively deposited BiOCl single-crystalline nanosheets could also degrade conventional pollutants like methyl orange, orange G, rhodamine B and salicylic acid (Fig. S18, ESI†), suggesting they are very promising for environmental applications.

Conclusions

In conclusion, high oxygen density characteristic of BiOCl {001} facets ensures the fast generation of oxygen vacancies in ethylene glycol under microwave irradiation, resulting in the in-situ nucleation and growth of Ag on electron-rich oxygen vacancies of {001} facets. The tight interfacial contact mode between Ag and {001} facets of BiOCl SCNSs arisen from oxygen vacancies induced selective silver deposition on {001} facets favors the SPR-excited electron transfer to {001} facets of BiOCl than the unselective Ag deposited counterparts, endowing Ag-BiOCl composites excellent reactivity on both Cr(VI) reduction and NaPCP oxidation under visible light. This study provides new physical insight into the relationship between the photocatalytic performances of the metal-semiconductor nanocomposites and the coupling modes of metal with certain facets of semiconductors, and also offers high performance plasmonic photocatalysts for efficient pollutant removal with solar energy.

Acknowledgements

This work was supported by National Basic Research Program of China (973 Program) (Grant 2013CB632402), National Science Foundation of China (Grant 21177048), Key Project of Natural Science Foundation of Hubei Province (Grant 2013CFA114), and Research Institute of Photocatalysis, State Key Laboratory of Photocatalysis on Energy and Environment.

Notes and references

Key Laboratory of Pesticide & Chemical Biology of Ministry of Education, Institute of Environmental Chemistry, College of Chemistry, Central China Normal University, Wuhan 430079, P. R. China. E-mail: zhanglz@mail.ccnu.edu.cn; Fax/Tel: +86-27-6786 7535

† Electronic Supplementary Information (ESI) available: [details of any supplementary information available should be included here]. See DOI: 10.1039/b000000x/

1 A. Capra, B. Scicolone, *Agric. Water Manage.*, 2004, **68**, 135.
2 N. L. Stock, J. Peller, K. Vinodgopal, P. V. Kamat, *Environ. Sci. Technol.*, 2000, **34**, 1747.
3 Z. H. Ai, W. K. HO, S. C. Lee, L. Z. Zhang, *Environ. Sci.Technol.*, 2009, **43**, 4143.
4 X. L. Hu, G. S. Li, J. C. Yu, *Langmuir*, 2010, **26**, 3031.
5 Y. Huang, W. Ho, Z. Ai, X. Song, L. Zhang, S. Lee, *Appl.Catal. B*, 2009, **89**, 398.
6 W. Li, D. Li, S. Meng, W. Chen, X. Fu, Y. Shao, *Environ. Sci. Technol.*, 2011, **7**, 2987.
7 X. F. Gao, W. T. Sun, Z. D. Hu, G. Ai, Y. L. Zhang, S. Feng, F. Li, L. M. Peng, *J. Phys. Chem. C*, 2009, **113**, 20481.
8 K. Awazu, M. Fujimaki, C. Rockstuhl, J. Tominaga, H. Murakami, Y. Ohki, N. Yoshida, T. Watanabe, *J. Am. Chem. Soc.*, 2008, **130**, 1676.
9 C. Gomes Silva, R. Juárez, T. Marino, R. Molinari and H. García, *J. Am. Chem. Soc.*, 2011, **133**, 595.
10 Y. Li, M. A. El-Sayed, *J. Phys. Chem. B*, 2001, **105**, 8938.
11 R. Narayanan, M. A. El-Sayed, *J. Am. Chem. Soc.*, 2003, **125**, 8340
12 L. D. Menard, F. Xu, R. G. Nuzzo, J. C. Yang, *J. Catal.*, 2006, **243**, 64.
13 (a) Z. K. Zheng, B. B. Huang, X. Y. Qin, X. Y. Zhang, Y. Dai, M. H. Whangbo, *J. Mater. Chem.*, 2011, **21**, 9079; (b) G. C. Xi, J. H. Ye, Q. Ma, N. Su, H. Bai, C. Wang, *J. Am. Chem. Soc.*, 2012, **134**, 6508.
14 X. Pan, Y. J. Xu, *Appl. Catal., A*, 2013, **459**, 34.

15 G. Liu, C. H. Sun, H. G. Yang, S. C. Smith, L. Z. Wang, G. Q. Lu, H. M. Cheng, *Chem. Commun.*, 2010, **46**, 755.

16 J. Jiang, K. Zhao, X. Y. Xiao, L. Z. Zhang, *J. Am. Chem. Soc.*, 2012, **134**, 4473.

17 K. Zhao, L. Z. Zhang, J. J. Wang, Q. X. Li, W. W. He, J. J. Yin, *J. Am. Chem. Soc.*, 2013, **135**, 15750.

18 C. D. Wagner, W. M. Riggs, L. E. Davis, J. F. Moulder, G. E. Muilenberg, in *Handbook of X-ray Photoelectron Spectroscopy, Physical Electronics Division*, Perkin-Elmer Corp., Eden Prairie, 1979.

19 (a) Y. Tian, T. Tatsuma, *J. Am. Chem. Soc.*, 2005, **127**, 7632; (b) J. He, I. Ichinose, T. Kunitake, A. Nakao, Y. Shiraishi, N. Toshima, *J. Am. Chem. Soc.*, 2003, **125**, 11034.

20 J. Jiang, L. Z. Zhang, H. Li, W. W. He, J. J. Yin, *Nanoscale*, 2013, **5**, 10573.

21 Skrabalak, L. Au, X. Li, Y. Xia, *Nat. Protoc.*, 2007, **2**, 2182.

22 M. Y. Xing, J. L. Zhang, F. Chen, B. Z. Tian, *Chem. Commun.*, 2011, **47**, 4947.

23 L. Q. Ye, L. Zan, L. H. Tian, T. Y. Peng, J. J. Zhang, *Chem. Commun.*, 2011, **47**, 6951.

24 G. H. Dong, L. Z. Zhang, *J. Phys. Chem. C*, 2013, **117**, 4062.